PERSPECTIVE

Check for updates

Supraballs as spherical solid 3D superlattices of hydrophobic nanocrystals dispersed in water: nanoarchitectonics and properties

M. P. Pileni [ID]

Herein, we use a water-dispersive 3D suprastructure of ferrite (Fe_3O_4) nanocrystals called supraballs. They are solid spherical assemblies of hydrophobic nanocrystals with a rather low Young's modulus compared to similar 3D superlattices deposited on a substrate. Using atomic force microscopy methods, their nanomechanical properties are measured, which show small flexibility and deformation. This suprastructure behaves as a nanoheater and remains self-assembled after internalization in cancer cells. Furthermore, when subjected to light, the percentage of dead cells compared to the nanocrystals used as building blocks and dispersed in the solution increases.

I. Introduction

In nature, materials are characterized by structural order over multiple length scales. They are often produced by self-assembly processes. These hierarchical design principles are ubiquitously used to maximize functionality from a limited choice of available components. Self-organization in colloidal suspensions leads to a fascinating range of beautiful crystalline structures and reveal more than just a pretty structure but also afford novel materials with collective and intrinsic properties.[1–11]

Pickering and Ramsden discovered that microsized solid particles stand at the interface between two immiscible fluids.[12] The assemblies of particles at the fluid interface induce a drop in the interfacial energy. When the particles are large (in the micrometer range), the thermal fluctuations are negligible. On decreasing the particle size to the nanometer range, the thermal fluctuations compete with the interfacial energy by a few k_BT. This gives rise to a rather weak nanoparticle confinement at the fluid interface. In such conditions, solid spherical confinement of hard spheres is produced in the oil-water emulsion.[13–16] Such colloidal self-assembled spherical confinements called "superballs/supraballs/supraparticles", subjected to geometric construction rules,[17] are produced with a large variety of building blocks such as ferrite nanocrystals, polymers, and silica colloids. In some cases, the crystalline structures are face centered-cubic (FCC) or icosahedral assemblies.[18] The solid spherical colloidal crystals are highly ordered with crystalline layers. Such supraballs are central to various fields of science and technology, ranging from colloidal chemistry and soft

matter physics to power technology and pharmaceutical and food sciences.[14]

In the last decades, nanomaterials have been designed for a range of biomedical applications, including diagnostics, gene and drug delivery, therapeutic applications for the treatment of cancer and infectious diseases, and regenerative medicine. However, the majority of administered nanomaterials are sequestered and, with time, get accumulated in organs such as the liver, which reduces their efficiency at their intended tissular, cellular or intracellular targets. Thus, one of the challenges of nanomedicine remains the tight control of nanomaterial interactions with the encountered biological environments.[19] For this reason, considerable effort has been made to understand how the size, shape, and material properties of the nanocarriers, and the interplay among these, affect cellular uptake.[20] The fate of nanoparticles once inside the cell is poorly controlled and understood.[21] This is unfortunate since the intracellular localization of nanoparticles will directly influence their biological effects. Most nanoparticles are internalized by endocytosis and converge to lysosomes. Upon the internalization of nanoparticles, cells continuously adapt their endosomal traffic and lysosome biogenesis in order to process them. However, the way lysosomes adapt to the presence and sequestration of nanomaterials, and whether such mechanisms depend on nanoparticle characteristics, remain elusive.[22] It must be emphasized that the precise localization, density, aggregation state, and organization of nanocrystals within intracellular compartments are of crucial importance for imaging and therapeutic applications. Furthermore, the proximity of nanoheaters to the lysosomal membrane has also been emphasized as a key requirement for the induction of cell death.[23] Photothermal therapy (PTT) has elicited new clinical trials as adjuvant or

Sorbonne Université Department of Chemistry, 4 Place Jussieu, 75005 Paris, France.
E-mail: mppileni@orange.fr; Web: https://supranano.wordpress.com

neo-adjuvant strategy to be applied in chemo-resistant and difficult-to-treat tumors that have to be reduced before surgery. Photoactivable nanomaterials including iron oxide nanoparticles[24] are remotely activated by a laser, which penetrates the tissue, generating controlled hyperthermia in the target region. Iron oxide nanocrystals are particularly attractive due to their natural meta-bolization by endogenous proteins, high biocompatibility, and clinical approval of several formulations that are combined with unique superparamagnetic properties for magnetic resonance imaging, photoacoustic tomography, magnetic manipulation, or magnetic hyperthermia as well as iron-related redox reactivity and ligh-to-heat conversion, whereas iron oxide nanocrystals are susceptible to both magnetic and light activation to produce local heating; the photothermal strategy has proved to be more efficient to induce tumor hyperthermia at low dosage.[25] In solid tumors, nanoparticles encountered not only tumor cells but different components of the tumor microenvironment that include stromal cells (among which we can find fibroblasts or immune cells) and a copious lattice of extracellular matrix. The intimate interactions of the nanomaterials with the hetero-geneous ecosystem of the tumor will dictate their tumor penetration, local distribution of nanoparticles, local heating efficiency, and the ultimate biological damages and mechan-isms of resistance that are induced. Nevertheless, little is known on how nanomaterials interact with the tumor micro-environment and how their structural properties can modulate these interactions, their heating capacity, and the PTT-induced biological outcomes. In particular, the use of self-assembled nanocrystals forming organized suprastructures is still a blank field despite their attractive properties.

In this perspective, we present supraballs of ferrite nano-crystals. These solid spheres are rather flexible with a rather low Young's modulus and act as "nanoheater". Furthermore, these supraballs can be internalized in the cancer cells, keeping their spherical structure and increasing their death when they are subjected to light.

II. Results and discussion

Supraballs are $\neq 150$ nm spherical self-assemblies of nanocrystals in fcc crystalline structure (Fig. 1).

To produce supraballs, we were inspired by the concept of "microreactor",[26] whose key feature was to transfer the hydro-phobic nanocrystals coated with aliphatic chain from the inner oil phase to the oil/water interface. Here, 10 nm Fe_3O_4 spherical nanocrystals with 6% size distribution are coated with the aliphatic ligand (oleic acid) produced from the thermal decom-position of iron oleate. With the emulsification of aqueous surfactant (i.e., dodecyltrimethylammonium bromide, DTAB) solution and the oil phase containing chloroform of Fe_3O_4 nanocrystals, these hydrophobic nanocrystals tend to adsorb on the droplet interface. This process is spontaneous and is driven by the sum of interfacial energy and the van der Waals interactions between the hydrophobic chains of the surfactant and the hydrophobic chain of the surface ligands anchored to
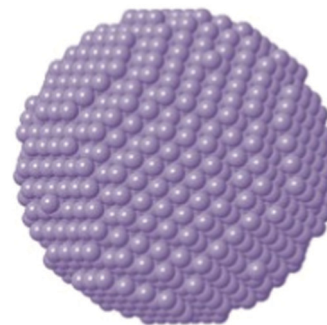

Fig. 1 Schematic of a supraball.

the nanocrystals. To stabilize the emulsion, ethylene glycol solution containing polyvinylpyrrolidone was added swiftly and stirred with a vortex. The emulsion was then heated under nitrogen atmosphere and kept at a constant temperature to evaporate the inner chloroform phase. The resulting nano-crystal assemblies were washed twice with ethanol and dis-persed in deionized water to form stable colloids.

To illustrate these nanocrystal assemblies in their native environment, Fig. 2a shows the cryo-transmission electron microscopy (cryo-TEM) image of typical spherical supraballs dispersed in water without any coalescence. In fact, these supraballs are highly stable for more than several years (>4) and do not show any collapse when suspended in water. After evaporation of the water solvent, two-dimensional (2D) TEM images were recorded on the TEM grid. Large spherical dense-packed assemblies of the nanocrystals were produced (Fig. 2b). These spherical assemblies were characterized by small-angle X-ray scattering (SAXS). Two typical rings indexed as {111} and {222} can be found in the SAXS pattern (inset in Fig. 2a), which indicate the face-centered cubic (FCC) packing mode. The supraball average diameter and size distribution are 100 nm and 30%, respectively.

The topographical image of a single FCC supraball deposited on a modified silica surface was obtained by atomic force microscopy (AFM) measurements;[27] Fig. 2d confirms the dia-meter of the supraball (100 nm) measured using an applied force of 2 nN. It is expected that the measured lateral supraball size is somewhat larger than its actual size due to tip-particle interactions. The supraball shape is almost spherical with a possible small deformation due to its attachment to the surface. The same supraball is scanned at higher imaging loads of 5 nN and 10 nN to evaluate the load dependence of the nanomechanical properties in water and to determine the ima-ging load limit, at which the irreversible shape changes and superstructure destruction occurs. No clear shape changes are observed at an imaging load of 5 nN, and this is also confirmed at a repeat scan over the same supraball using the same load. However, an indication of irreversible shape changes of the supraball is observed at the imaging force of 10 nN, where the upper edge of the supraball appears to be suppressed or cut. Thus, the imaging loads of 2 nN and 5 nN are regarded as safe for the studies of these supraballs in aqueous media.
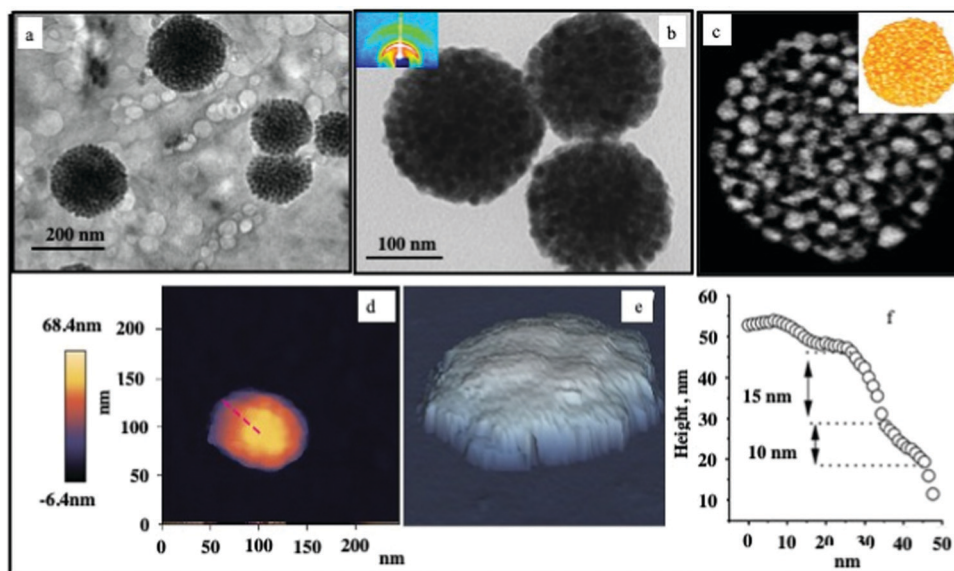
Fig. 2 (a) CryoTEM in water, (b) TEM image, (c) 2D HAADF–STEM projection image of the dried sample; inset: 3D tomogram. (d) Topography image of a single fcc supraball measured at 2 nN. (e) The corresponding 3D image to highlight the step-like surface structure. (f) The corresponding 3D image to highlight the step-like surface structure.

The deformation increases with increasing applied load. This confirms that such FCC supraballs can deform and then relax to their original shape. The deformation is assigned to the presence of the coating material. This is supported by the presence of more deformable regions between the less deformable primary nanocrystals. The supraball deformation at 10 nN reaches about half the value of its height measured at the given applied load. This suggests that, at and about 10 nN, the supraball cannot be further deformed and that at this and higher forces, plastic deformation leading to permanent shape changes occurs.

The change in the TEM image contrast has a characteristic feature due to the step-edge structure of the assembled nanocrystals (Fig. 2b). This is confirmed from the AFM image shown in (Fig. 2e). The color bar variation in Fig. 2d is chosen to highlight the layered structure in the hybrid materials, and this layered structure is also clearly shown in the 3D topography images in Fig. 2e. The height of the step edges between the nanocrystal layers was quantified by analyzing the height cross-section. Here, steps of about 10–15 nm are obtained, which is consistent with the size of the nanocrystal (10 nm) and the associated organic coating.

A layered structure is noticeable in the topographical image, as illustrated in Fig. 3a. The deformation (Fig. 3b) and adhesion (Fig. 3c) maps highlight the changes in the thin, few nm edge region. This is expected considering that organic molecules (oleic acid and DTAB) encapsulate the nanocrystals. The existence of such chemicals on the surface and in between the nanocrystals increase the adhesion forces and the deformation at these locations, as shown in Fig. 3c. The local changes in deformation and adhesion are correlated with height changes along cross-sections, as shown in Fig. 3d.

The small edge steps of about 10 nm for the layers of nanocrystals are visible, as also illustrated in Fig. 2d–f. The adhesion force data show only a small increase in the edge region and very little variation at the step edges. It should be noted that the adhesion force depends on the contact area and is likely to contribute to the increased adhesion at the edges. Similar step edge structures were already observed for FCC cobalt iron oxide[28] or colloidal silica particles.[11] Note that an increase in elastic modulus and stiffness with increasing load is uniform (Fig. 4).

Instead of studying the mechanical properties of a single fcc supraball deposited on a modified silica surface and imaged in water, let us consider a supraball dried on a mica substrate in air.[29] The supraball image has a sharper contrast, and all individual nanocrystals are clearly visible (Fig. 5a). This can be attributed to the dense nanocrystal packing. The adhesion force maps show higher adhesion in the edge region of the supraballs (Fig. 5b). This is due to the larger contact area of the organic coating with the tip at the edges. Contrary to the stiffness maps (Fig. 5c), which provide a model-free mechanical property, the apparent elastic modulus maps (Fig. 5d) provide a somewhat model-dependent but more common measure of the mechanical response. The variation in elastic modulus along the supraball shows a higher modulus on top of the nanocrystals and lower in between the nanocrystals. This variation is due to a lower mobility of the nanocrystals during their interaction with the probing AFM tip. In the central region, the average adhesion force, elastic modulus, and stiffness are 5.4 ± 0.5 nN, 7.9 ± 2.2 GPA, and 53.6 ± 6 N m^{-1}, respectively. The data described in a dry system are in very good agreement to those already obtained with a large variety of 3D superlattices deposited on a substrate.[30]

The data presented above are obtained from the same batch of supraballs. Hence, the difference is related to the environment with supraball deposition on either a mica substrate
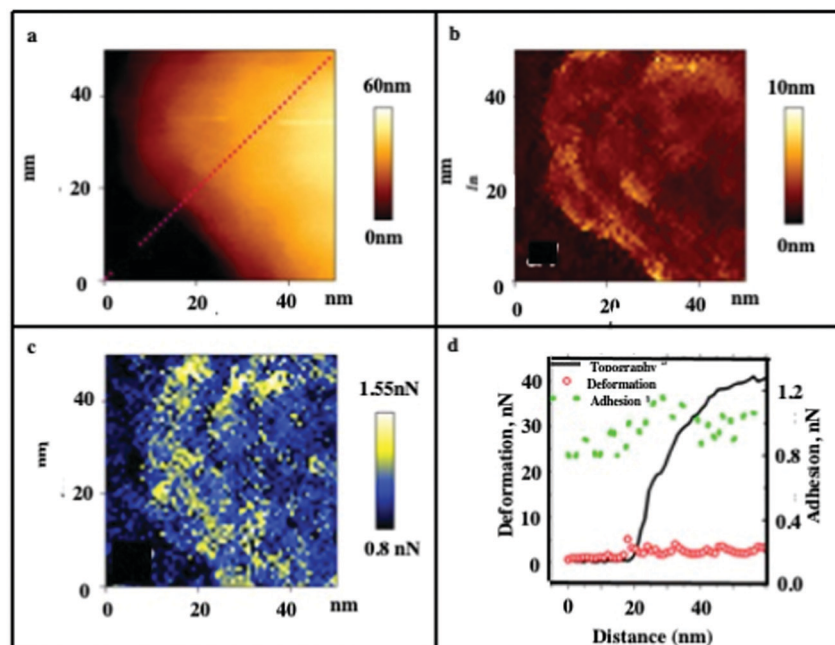
14142 | Phys. Chem. Chem. Phys., 2022, 24, 14140–14149

This journal is © the Owner Societies 2022

Fig. 3 High-resolution topography images measured at the edge of a single FCC supraball using an imaging load of 2 nN in water using AFM in the QI mode. The corresponding high-resolution data for deformation are shown in (a), and for adhesion force in (b). The cross-section data for topography, adhesion and deformation taken along the red dash lines (a) are shown in (c). The y-axis in (d) is for both deformation and height.
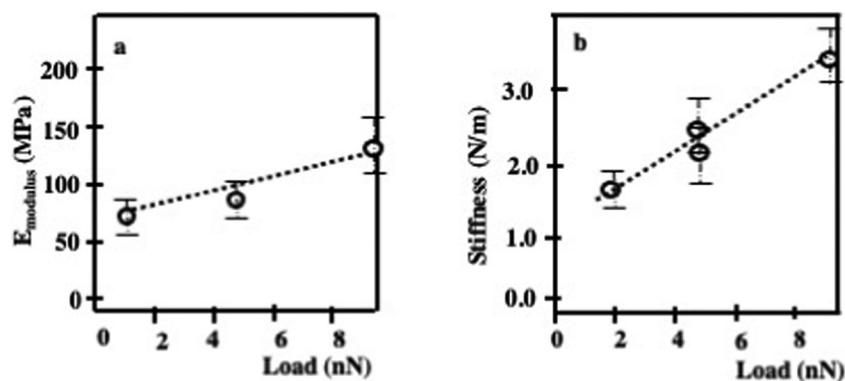

Fig. 4 The load-dependence of (a) the elastic modulus and (b) stiffness of a single supraball. The error bars represent property variations for each studied hybrid. The values were confirmed for some more hybrid particles at the same loads.

(dry system) or a modified silica surface in water environment. This permits to conclude that the environment modifies the nanomechanical properties of supraballs. These low values of the Young's moduli have to be attributed to the environment and, more specifically, to the water surrounding the supraballs, as already observed with nanoparticles synthesized for therapeutics and attributed to surface alteration.[31]

Unexpectedly, with no obvious explanation, the supraball absorption spectrum considerably drops as compared to that of its building blocks (Fig. 6). By ethanol addition into the colloidal solution, after some time, the supraball structure progressively disappears and the absorption of dispersed nanocrystals is recovered. This clearly shows that the drop of the supraball absorption is related to the formation of 3D photonic crystals.[32,33]

The energy flow upon light irradiation is investigated by pump-probe experiments.[35] The differential transmission ($\Delta T/T$) spectra are recorded as a function of time and the probe wavelength, λ. At the initial time scale of ten picoseconds, the typical $\Delta T/T$ map is attributed to the transient spectra of the dispersed nanocrystals at various probe wavelengths. This spectrum exhibits a decay constant of few picoseconds (Fig. 7a). It is attributed to the timescale of electron-phonon scattering. Such dynamic data confirms that Fe_3O_4 supraballs at room temperature retain the fingerprint of the dispersed nanocrystals used as building blocks.

At longer time scales, the $\Delta T/T$ map of supraballs (Fig. 7b) exhibit *very distinct features*. Instead of a monotonic decrease over time, we observed the build-up of a positive signal, which is red-shifted by about 100 nm compared to the earlier spectra.
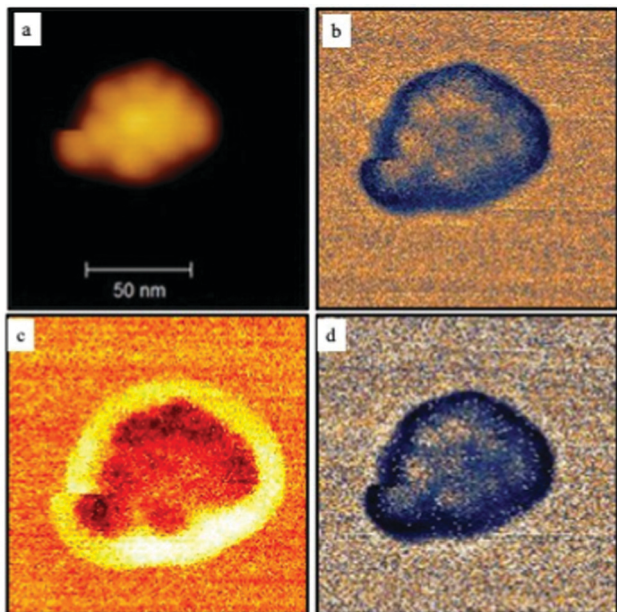
Fig. 5 Scanning probe microscopy results of one single supraball. (a) Topography, (b) adhesion, (c) stiffness, and (d) elastic modulus using the QI mode with SPM.
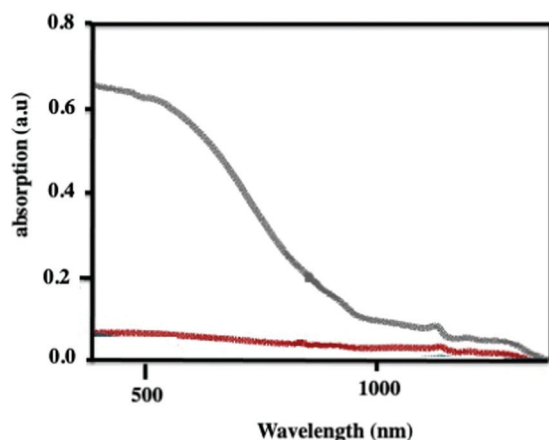

Fig. 6 Vis-NIR absorption spectra of Fe_3O_4 nanocrystals either dispersed (black) or self-assembled to the produced supraballs (red). Reprinted with permission from ref. 34. Copyright 2020 John Wiley & Sons, Inc.

This novel phenomenon cannot be ascribed to mechanical oscillations.[36] Similar data were obtained with Au supracrystals dispersed in aqueous solution. To explain the origin of such unexpected transient optical response at the long timescale that remain constant at the nanosecond time scale, a model to simulate the optical experiments was developed.[35] Due to the high penetration depth of light in the supraball structure (about 60 nm), despite the thickness of the assembly, the power absorbs per unit volume is more uniform compared with that in a nanosphere of the same diameter. The pump pulse is absorbed by the metallic oxide phase of the supraballs and initiates a chain of energy transfer processes. According to this model, the delayed build-up of the $\Delta T/T$ signal on the

few hundred picoseconds timescale is the signature of the final step in the light-heat conversion process that ultimately results in the heating of the matrix of organic ligands. With Au supracrystals, a very good agreement between the experiments and the model confirms a collective regime of photo-temperature generation enabled by the assembling. It is concluded that the coating agent, even though not directly absorbing, acts as an internal reservoir for the efficient accumulation of the energy within few hundreds of picoseconds. Very surprisingly, without any simple explanation, such long-time scale transient has *never been observed in dried systems*, *i.e.*, when the corresponding untreated supracrystals are deposited in a substrate. Similar behavior, as observed with supraballs and Au "clustered" structures, are obtained with colloidosomes, which are "eggs" structures that make such assemblies universal "nanoheaters" when they are subjected to light.

The zeta potential of the dispersed nanocrystals coated with dopamine and that of supraballs dispersed in deionized water are +48 mV and +46 mV, respectively. The similarity between these various values clearly indicates that the zeta potential has a negligible influence on the data presented below.

We investigated the interactions of A431 epidermoid carcinoma cells with supraballs and their building blocks dispersed in water.[29] The cells were exposed to the nanomaterials in serum-complemented culture medium for one day. No sign of nanocrystal aggregation in the culture medium was observed. None of the nanocarriers presented cytotoxicity at concentration [Fe] 27 μg mL^{-1}, as assessed by the metabolic activity measurements that were similar to the control non-exposed cells. Consistently, the necrosis level does not exceed 7% in all conditions.

In order to elucidate the intracellular distribution and fate of nanocrystals in tumor cells, we followed the particle's uptake by TEM at one day after exposure to the nanostructures. Dopamine-coated isolated Fe_3O_4 nanocrystals interact early as loose clusters with the cell plasma membrane and are promptly internalized into the membrane-closed endosomes, in which their relatively dispersed state is preserved (Fig. 8a). Supraballs collectively interact with the plasma membrane at short times, mostly conserving their spherical structure after entering intracellular compartments (Fig. 8b). Note that the supraball structures conserve a locally ordered organization within the cell compartment.

The diameter of nanocrystals before and after internalization remains unchanged for Fe_3O_4 nanocrystals dispersed in aqueous solution (Fig. 9a and b), whereas an increase in the supraball diameter and size distribution are observed after 1 day incubation (Fig. 9c and d). However, after entering the cell, the apparent size and size distribution do not change, demonstrating that the reorganization mostly occurred at early times. Hence, such an increase in the supraball size could be explained as follows: during the internalization process, some interaction between nanocrystals and biological membrane takes place. As soon as the nanocrystals are internalized, specific interaction between nanocrystals having same coating agent favor their association with the supraball core.
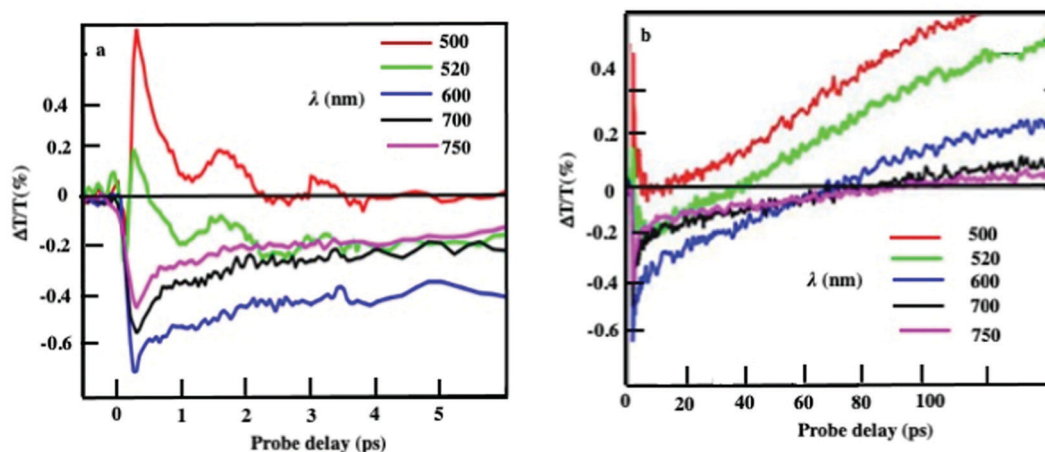
Fig. 7 Dynamics of the $\Delta T/T$ at selected probe wavelengths at short (a) and long (b) time scales of the supraballs. Reprinted with permission from ref. 35. Copyright 2019 National Academy of Sciences.
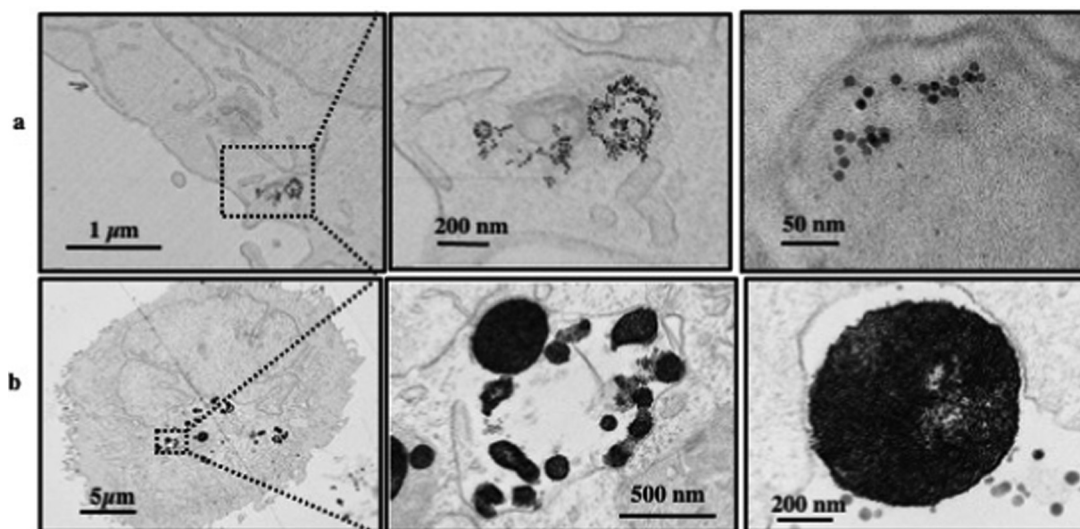

Fig. 8 2D TEM slice images at various enhancements of dispersed Fe_3O_4 nanocrystals (a) and supraballs (b) in A431 tumor cells incubated for 1 day with 28 μg mL^{-1} iron concentration.

In order to investigate the average structural organization and integrity of nanocrystals in cells with high-statistics, we carried out small angle X-ray scattering (SAXS) experiments at different time-points from 30 min to 2 days during the cell processing of isolated nanocrystals and supraballs. The contribution of nanocrystals is obtained by subtracting the scattered intensity of non-labelled cells to the overall scatter. The SAXS patterns, at high q, fit the form factor $P(q)$ of the spheres with diameter of about 10 nm, which is in line with the cryoTEM size and spherical shape of individual nanocrystals. The structure factor $S(q)$, obtained by dividing the scattered intensity by the form factor $P(q)$ of individual nanocrystals, provides (at low q) information on the local organization of the nanocrystals. For cells incubated with isolated nanocrystals, the structure factor at low q is characterized by a power law decay with an exponent of -1.7 (Fig. 10a).

This indicates the cell-induced formation of nanocrystal aggregates with an open structure and an increase in the aggregation number. This intracellular fractal aggregation of nanocrystals, similar to diffusion-limited aggregation, is fully consistent with the TEM observations reported above and with previous small angle neutron scattering results on endosomal clustering of iron oxide nanoparticles.[37] For cells incubated with supraballs, the structure factor is characterized by a power law decrease of the scattered intensity with an exponent of -2.9 (Fig. 10b), demonstrating a dense packing of the nanocrystals.

Taken together, in the SAXS and TEM structural analysis, we claim that isolated nanocrystals are internalized in the form of loose fractal aggregates, whereas the local organization of pre-assembled nanocrystals into supraballs persists in cell organelles. This might be explained by the hydrophobic coating
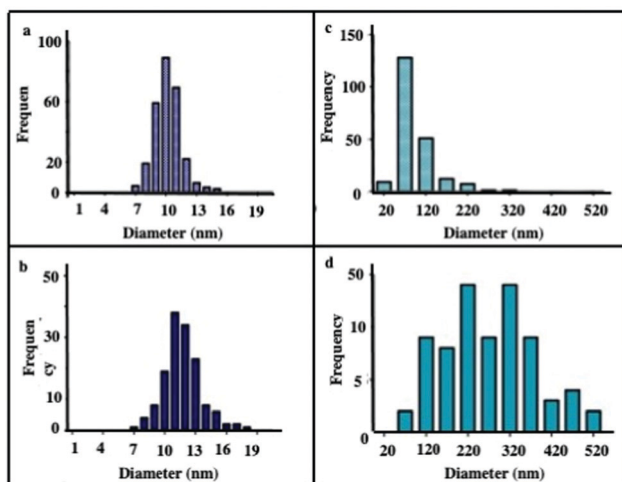
This journal is © the Owner Societies 2022

Phys. Chem. Chem. Phys., 2022, **24**, 14140–14149 | **14145**

Fig. 9 Histograms of dispersed nanocrystals and supraball diameters (a and c) detected by cryoTEM and (b and d) from the 2D TEM slices of A341 cells at 1 day, following incubation with 28 μg mL^{-1} iron.

agents of the nanocrystals that maintain the attractive interactions between the nanocrystals in the hydrophilic medium.

As shown above, in the analogy with the data obtained with Au "clustered" structures, such supraballs act as nanoheaters. Here, an opportunity is open to evaluate their abilities in favoring the cancer cell damages. For the photo-induced heating properties of Fe_3O_4 nanocrystals and supraballs, we need to compare the absorption spectra of the supraballs and dispersed Fe_3O_4 nanocrystals in aqueous solution. As shown on Fig. 6, a drop in the absorption spectrum of the supraballs is observed compared to their building blocks. The photo-activated heating of the supraballs or dispersed Fe_3O_4 nanocrystals was obtained by subjecting 100 μL of the suspension at a fixed iron concentration (150 μg mL^{-1}) to an 808 nm laser power (1 W cm^{-2}) for 5 min. The temperature increase is the largest for supraballs (10.9 °C), followed by Fe_3O_4 nanocrystals (8.8 °C). According to the drop in the suprastructure absorption spectra compared to that of dispersed Fe_3O_4 nanocrystals, we could expect a lower temperature increase for supraballs compared to Fe_3O_4 nanocrystals. The relative increase in the thermal increment of the supraballs compared to dispersed nanocrystals could be related to the fact that supraballs act as nanoheaters.[35]

Below, we will consider either the global or local photothermal damages.

Let us first consider the global heating efficiency. A431 human epidermoid carcinoma cells are incubated with either the dispersed building blocks or supraballs at an iron concentration of 28 μg mL^{-1} for one day. The cells were then washed carefully to discard the excess Fe_3O_4 nanocrystals that had not been internalized, and one million cells were pelleted and resuspended in 100 μL of the culture medium before irradiation with an 808 nm laser in the same experimental conditions as for the nanostructures in the suspension. Dispersed Fe_3O_4 nanocrystals heating efficiency is significantly higher to that of the supraballs once internalized in cells. From an initial temperature of 25 °C, cells reach a plateau temperature of 38.4 °C and 33.5 °C for Fe_3O_4 nanocrystals and supraballs, respectively. From that, we conclude that the global heating remains similar with supraballs and dispersed nanocrystals.

To identify cell apoptosis and necrosis, fluorescent dyes are used; Hoechst 33342 allows the quantification of all cells (blue), YO-PRO^{TM} dye can enter cells under apoptosis (green), whilst propidium iodide (red) cannot, and it only stains dead necrotic cells. From previous studies,[38,39] we know that the local thermal damages induced in the vicinity of the heat nanosources is much higher than the macroscopic temperature in the surrounding medium. For this purpose, we concentrate on the local potential effects of intracellular heating. Hence, cell monolayers having internalized either dispersed Fe_3O_4 nanocrystals or supraballs were exposed to the laser and cell death was quantified. Fig. 11 shows that cells, having internalized, the two structures without laser irradiation did not show any significant enhancement in the apoptosis or necrosis level in comparison to the control cells, irradiated or not, showing that neither nanocrystal nor laser exposure affects the cell viability itself. Cells having internalized dispersed Fe_3O_4 nanocrystals show slightly enhanced levels of apoptosis and necrosis after irradiation, but the difference with the non-irradiated cells is not statistically significant. In contrast, supraball-loaded cells feature a significant enhancement of the apoptosis and necrosis level after irradiation. For supraballs, the percentage of cell damages is 58% (40% necrosis + 18% apotheosis), whereas it is 35% (30% necrosis + 5% apotheosis) for dispersed nanocrystals. This clearly demonstrates that supraballs internalized
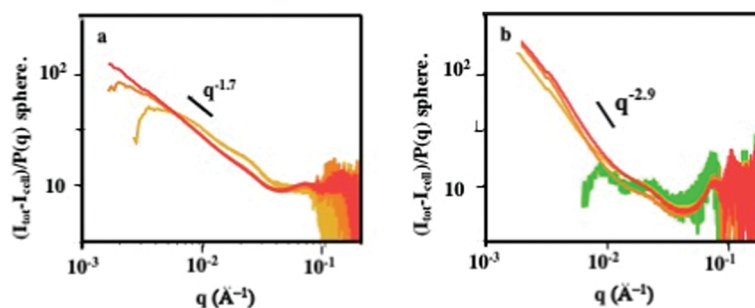

Fig. 10 Structure factor, $S(q)$, of the nanocrystals embedded in cells incubated with nanocrystals (a) and supraballs (b) at the different time points (30 min (green), 4 hours (yellow), 1 day (orange) and 2 days (red)).
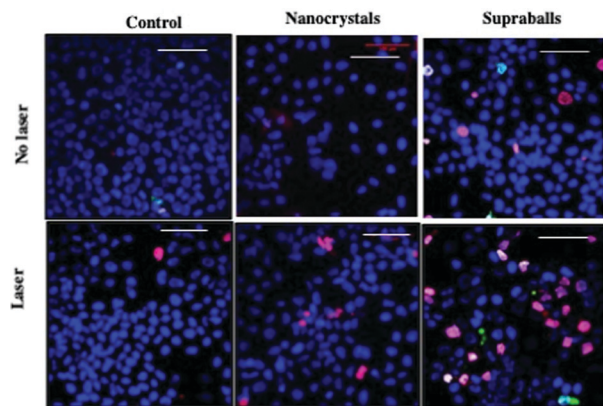
14146 | *Phys. Chem. Chem. Phys.*, 2022, **24**, 14140–14149

This journal is © the Owner Societies 2022

Fig. 11 Evaluation of the local cellular damage induced by Fe$_3$O$_4$ nanocrystals and supraball-mediated PTT in cell monolayers 4 h post-irradiation. Representative fluorescence images of A431 cells. Cells were stained with Hoechst 33342 (cell nuclei, blue), YO-PRO^{TM} (apoptotic cells) and propidium iodide (necrotic cells). Scale bar = 50 μm.

by cells induce local damages, which provokes cell apoptosis and necrosis without the global heating of the environment. These results are surprising considering the lower global temperature of the cell pellet for supraballs in comparison to Fe$_3$O$_4$ nanocrystals. Hence, dispersed Fe$_3$O$_4$ nanocrystals, despite exhibiting higher heating efficiency both in aqueous solution and in the cell pellet, induce less cellular damage upon the irradiation of the cell monolayers. This has to be related to the fact that, as demonstrated above, the light absorption in such supraballs, dispersed in aqueous solution, initiates a chain energy transfer, having various degrees of freedom coupled together.

III. Conclusion

Herein, we used water/oil interface as a template to self-assemble hydrophobic nanocrystals in spherical solid supraballs dispersed in aqueous solution as atomic clusters.[40] The physical properties of the solid spherical suprastructure remain at the early stage. However, some of those can be assigned—the absorption spectrum of these supraballs dispersed in aqueous solution markedly drop compared to their building blocks dispersed in solution, which is the signature of a photonic crystal. Some simulations are needed for a better understanding. The mechanical properties of supraballs deposited on modified silica surface are characterized by a rather low Young's modulus compared to similar assemblies deposited on a substrate. Furthermore, slight adhesion and deformation are observed at the step edge of the supraballs. A rather low load is needed to deform the suprastructure. When it is subjected to light, it acts as nanoheaters. The supraball cellular uptake markedly increases in a cell model of human epidermoid carcinoma (A431). Furthermore, the supraballs maintain the solid spherical structure before and after internalization with a slight increase in the size distribution. The photothermal effect induces extended tumor necrosis after laser exposure.

IV. Perspectives

Over these last two decades, the self-assembly of nanocrystals into hierarchical structures, considered as novel materials, was widely investigated. A large variety of crystalline structures has been reported with the production of 3D superlattices with either low or high index surfaces, quasi crystals, negative crystals, *etc.* Furthermore, we know that such assemblies are characterized by a large number of collective and intrinsic properties (optical, magnetic, mechanical, *etc.*).[1–11]

Here, this suprastructure combines the collective and intrinsic properties to the new ones. This opens a large potential application. Let us list some of these physical properties. From previous studies, we know that such a suprastructure acts as a photonic crystal.[41] When supraballs are subjected to light, due to the dilution of the metallic phase, the penetration depth of visible light is greater than that in homogeneous metallic nanocrystals of a similar size, and they can be considered as nanoheaters. Furthermore, we have to remember that the building blocks of nanocrystals of such supraballs are magnetic nanocrystals and they are highly stable and dispersed in aqueous solution. This clearly indicates that such colloidal assemblies could be associated with ferrofluids having intrinsic magnetic, optical, and thermal properties. This opens a large number of potential applications. To name a few, with enhanced thermal conductivity, the possibility of external control, and manipulation of heat transfer coefficient, supraballs compete with other standard heat transfer solutions. In biomedicine, we show that supraballs are efficient for killing the tumor cells. Other potentialities can be proposed: they can be assimilated to a new tracer imaging that is gaining significant interest from the scientific community. This involves superparamagnetic contrast agents for the magnetic resonance of blood vessels for cell tracking as a tool until one cell therapy becomes mainstream. Such supraballs are useful for humans than iodine or gadolinium, which are usually used. As already mentioned, such supraballs are central steps in various fields of science and technology, ranging from colloidal chemistry and soft matter physics to power technology, pharmaceuticals, and food sciences.

Conflicts of interest

There are no conflicts to declare.

Acknowledgements

References

1 M. P. Pileni, Nanocrystals self-assemblies: fabrication and collective properties, *J. Phys. Chem.*, 2001, **105**, 3358–3372.

This journal is © the Owner Societies 2022

Phys. Chem. Chem. Phys., 2022, **24**, 14140–14149 | **14147**

2 M. P. Pileni, Self-assembly of inorganic nanocrystals: fabrication and collective intrinsic properties, *Acc. Chem. Res.*, 2007, **40**, 685–693.

3 A. Zabet-Khosousi and A.-A. Dhirani, Charge Transport in Nanoparticle Assemblies, *Chem. Rev.*, 2008, **108**, 4072–4124.

4 M. P. Pileni, Supra and Nano crystallinity: specific properties related to crystal growth mechanisms and nanocrystallinity, *Acc. Chem. Res.*, 2012, **45**, 1965–1972.

5 P. F. Damasceno, M. Engel and S. C. Glotzer, Predictive self-assembly of polyhedra into complex structures, *Science*, 2012, **337**, 453–457.

6 M. A. Boles, M. Engel and D. V. Talapin, Self-Assembly of Colloidal Nanocrystals: From Intricate Structures to Functional Materials, *Chem. Rev.*, 2016, **116**, 11220–11289.

7 M. P. Pileni, Impact of the metallic crystalline structure on the properties of nanocrystals and their mesoscopic assemblies, *Acc. Chem. Res.*, 2017, **50**, 1946–1955.

8 S. Alizadeh and Z. Nazari, A Review on Gold Nanoparticles Aggregation and Its Applications, *J. Chem. Rev.*, 2020, **2**, 228–242.

9 C. Yan, H. Portalès, N. Goubet, I. Arfaoui, S. Sirotkin, A. Mermet and M. P. Pileni, Assessing the Relevance of Building Block Crystallinity for Tuning the Stiffness of Gold Nanocrystal Superlattices, *Nanoscale*, 2013, **5**, 9523–9527.

10 I. D. Hosein, S. H. Lee and C. M. Liddell, Dimer-based three-dimensional photonic crystals, *Adv. Funct. Mater.*, 2010, **20**, 3085–3091.

11 J. D. Forster, *et al.*, Assembly of optical-scale dumbbells into dense photonic crystals, *ACS Nano*, 2011, **5**, 6695.

12 S. U. Pickering, Emulsions, *J. Chem. Soc., Trans.*, 1907, **91**, 2001–2021.

13 J. Zhuang, H. Wu, Y. Yang and T. C. Cao, Supercrystalline Colloidal Particles from Artificial Atoms, *J. Am. Chem. Soc.*, 2007, **129**, 14166–14167.

14 F. Montanarella, *et al.*, Crystallization of nanocrystals in spherical confinement probed by in situ X-ray scattering, *Nano Lett.*, 2018, **18**, 3675–3681.

15 B. de Nijs, S. Dussi, F. Smallenburg, J. D. Meeldijk, D. J. Groenendijk, L. Filion, A. Imhof, A. van Blaaderen and M. Dijkstra, Entropy-driven formation of large icosahedral colloidal clusters by spherical confinement, *Nat. Mater.*, 2015, **14**, 56–60.

16 L. Rossi, V. Soni, D. J. Ashton, D. J. Pine, A. P. Philipse, P. M. Chaikin, M. Dijkstra, S. Sacanna and W. T.-M. Irvine, Shape-sensitive crystallization in colloidal superball fluids, *Proc. Natl. Acad. Sci. U. S. A.*, 2015, **112**, 5286–5290.

17 J. Wang, C. F. Mbah, T. Przybilla, S. Englisch, E. Spiecker, M. Engel and N. Nicolas Vogel, Free Energy Landscape of Colloidal Clusters in Spherical Confinement, *ACS Nano*, 2019, **13**, 9005.

18 S. Disch, E. Wetterskog, R. P. Hermann, D. Korolkov, P. Busch, P. Boesecke, O. Lyon, U. Vainio, G. Salazar-Alvarez, L. Bergström and T. Brückel, Structural diversity in iron oxide nanoparticle assemblies as directed by particle morphology and orientation, *Nanoscale*, 2013, **5**, 3969–3975.

19 S. Wilhelm, A. J. Tavares, Q. Dai, S. Ohta, J. Audet, H. F. Dvorak and W. C. Chan, Analysis of nanoparticle delivery to tumours, *Nat. Rev. Mater.*, 2016, **1**, 16014.

20 A. C. Anselmo, M. Zhang, S. Kumar, D. R. Vogus, S. Menegatti, M. E. Helgeson and S. Mitragotri, Elasticity of nanoparticles influences their blood circulation, phagocytosis, endocytosis, and targeting, *ACS Nano*, 2015, **9**, 3169–3177.

21 R. Hartmann, M. Weidenbach, M. Neubauer, A. Fery and W. J. Parak, Stiffness-Dependent In Vitro Uptake and Lysosomal Acidification of Colloidal Particles, *Angew. Chem., Int. Ed.*, 2015, **54**(4), 1365–1368.

22 W. Song, S. Lee, S. Savini, M. Popp, L. Colvin and V. L. Segatori, Ceria Nanoparticles Stabilized by Organic Surface Coatings Activate the Lysosome- Autophagy System and Enhance Autophagic Clearance, *ACS Nano*, 2014, **8**(10), 10328–10342.

23 M. Pérez-Hernández, P. del Pino, S. G. Mitchell, M. Moros, G. Stepien, B. Pelaz, W. J. Parak, E. M. Gálvez, J. Pardo and J. S.-M. de la Fuente, Dissecting the Molecular Mechanism of Apoptosis during Photothermal Therapy Using Gold Nanoprisms, *ACS Nano*, 2014, **9**, 52–61.

24 R. Das, N. Rinaldi-Montes, J. Alonso, Z. Amghouz, E. Garaio, J. A. Garcia, P. Gorria, J. A. Blanco, M. H. Phan and H. Srikanth, Boosted Hyperthermia Therapy by Combined AC Magnetic and Photothermal Exposures in Ag/Fe$_3$O$_4$ Nanoflowers, *ACS Appl. Mater. Interfaces*, 2016, **8**(38), 25162–25169.

25 Z. Zijian Zhou, R. Rui Tian, Z. Wang, Z. Zhen Yang, Y. Liu, G. Liu, R. Wang, J. Gao, J. Song, L. Nie and X. Chen, Artificial local magnetic field inhomogeneity enhances, *Nat. Commun.*, 2017, **15468**, 1–4.

26 M. P. Pileni, Reverse micelles: a microreactors, *J. Phys. Chem.*, 1993, **97**, 6961–6974.

27 I. Dobryden, Z. Yang, P. M. Claesson and M. P. Pileni, Water Dispersive Suprastructures: An Organizational Impact on Nanomechanical Properties, *Adv. Mater. Interfaces*, 2020, **8**, 2001687.

28 B. de Nijs, S. Dussi, F. Smallenburg, J. D. Meeldijk, D. J. Groenendijk, L. Filion, A. Imhof, A. van Blaaderen and M. Dijkstra, Entropy-driven formation of large icosahedral colloidal clusters by spherical confinement, *Nat. Mater.*, 2014, **14**, 56.

29 A. Nicolas-Boluda, Z. Yang, I. Dobryden, F. Carn, N. Winckelmans, C. Pechoux, P. Bonville, S. Bals, P. M. Claesson, F. Gazeau and M. P. Pileni, Intracellular Fate of Hydrophobic Nanocrystal Self-Assemblies in Tumor Cells, *Adv. Funct. Mater.*, 2020, **30**, 2004274.

30 M. P. Pileni, Mechanical properties of supracrystals, *Eur. Phys. Lett.*, 2017, **119**, 37002.

31 T. Kulkarni, D. Mukhopadhyay and S. Bhattacharya, Influence of surface moieties on nanomechanical properties of gold nanoparticles using atomic force microscopy, *Appl. Surf. Sci.*, 2022, **591**, 153175.

32 K. Ishizaki, K. Suzuki and S. Noda, Fabrication of 3D Photonic Crystals toward Arbitrary Manipulation of Photons in Three Dimensions, *Photonics*, 2016, **3**, 36.

33 R. B. Wehrspohn and J. Upping, 3D photonic crystals for photon management in solar cells, *J. Opt.*, 2012, **14**, 024003.

14148 | *Phys. Chem. Chem. Phys.*, 2022, **24**, 14140–14149

This journal is © the Owner Societies 2022

34 A. Nicolas-Boluda, Z. Yang, T. Guilbern, L. Fouassier, F. Carn, F. Gazeau and M. P. Pileni, Self-Assemblies of Fe_3O_4 Nano-crystals: Toward Nanoscale Precision of Photothermal Effects in the Tumor Microenvironment, *Adv. Funct. Mater.*, 2020, **31**, 2006824.

35 A. Mazzanti, Z. Yang, M. G. Silva, N. Yang, G. Rizza, P. E. Coulon, C. Manzoni, A. M. de Paula, G. Cerullo, G. Della Valle and M. P. Pileni, Light–heat conversion dynamics in highly diversified water-dispersed hydrophobic nanocrystal assemblies, *Proc. Natl. Acad. Sci. U. S. A.*, 2019, **116**, 8161–8166.

36 G. V. Hartland, Optical studies of dynamics in noble metal nanostructures, *Chem. Rev.*, 2011, **111**, 3858–3887.

37 C. Rivière, C. Wilhelm, F. Cousin, V. Dupuis, F. Gazeau and R. Perzynski, Internal structure of magnetic endosomes, *Eur. Phys. J.*, 2007, **22**, 1–10.

38 J. T. Dias, M. Mros, P. del Pino, S. Rivera, V. Grazu and J. M. de la Fuente, DNA as a Molecular Local Thermal Probe for the Analysis of Magnetic Hyperthermia, *Angew. Chem., Int. Ed.*, 2013, **52**, 11526–11529.

39 A. Riedinger, P. Guardia, A. Curcio, M. A. Garcia, R. Cingolani, L. Manna and T. Pellegrino, Subnanometer Local Temperature Probing and Remotely Controlled Drug Release Based on Azo-Functionalized Iron Oxide Nanoparticles, *Nano Lett.*, 2013, **13**, 2399–2406.

40 J. Lacava, P. Born and T. Kraus, Nanoparticle Clusters with Lennard-Jones Geometries, *Nano Lett.*, 2012, **12**(6), 3279.

41 N. Vogel, S. Stefanie Utech, G. T. England, T. Shirman, K. R. Phillips, N. Koay, I. B. Burgess, M. Kolle, D. A. Weitz and J. Aizenberg, Color from hierarchy: diverse optical properties of micron-sized spherical colloidal assemblies, *Proc. Natl. Acad. Sci. U. S. A.*, 2015, **112**, 10845–10850.